Effect of Ca^{2+} Position in Zeolite Y on Selective Oxidation of Propane at Room Temperature

Jiang Xu, Barbara L. Mojet, Jan G. van Ommen, and Leon Lefferts*

Catalytic Processes and Materials, Faculty of Science and Technology, Institute of Mechanics Processes and Control Twente (IMPACT), University of Twente, P.O. Box 217, 7500 AE, Enschede, The Netherlands

Received: March 26, 2004; In Final Form: June 8, 2004

The activity of CaNaY zeolites in selective oxidation of propane with increasing Ca^{2+} content at room temperature was studied with infrared spectroscopy and ammonia temperature-programmed desorption. Increasing the Ca^{2+} exchange level in CaNaY zeolites resulted in a variety of altered properties: the amount of Brönsted and Lewis acid sites increased, the adsorption of propane increased, the initial acetone formation rate increased, and the desorption of acetone retarded. Moreover, all of these properties showed a sudden change with Ca^{2+} content above the 50% Na^+ exchange level, which can be fully attributed to the location of Ca^{2+} in the Y-zeolite framework. It is convincingly shown that only Ca^{2+} ions located in the supercage contribute to the formation of Brönsted and Lewis acidity as well as propane oxidation activity at room temperature.

Introduction

Zeolites belong to a large family of (alumino)silicates constituted by corner-linked TO_4 tetrahedra (T represents either Al or Si) that adopt a remarkable variety of crystalline structures containing channels and/or cavities with different dimensions.[1−4] Aluminum-containing zeolites have a negatively charged framework which results from AlO_2^- units replacing neutral SiO_2 units. The negative charge is balanced by an equivalent number of extraframework cations, often alkali or alkaline-earth metal cations. Zeolite Y is the synthetic form of faujasite and has a Si/Al ratio between 2 and 5. Its framework has two main cages: the large supercage results from an assembly of the basic units, the sodalite cages (Figure 1). The spherical supercages are approximately 13 Å in diameter. Access to supercages is afforded by four 12-membered ring windows about 9 Å in diameter, which are tetrahedrally distributed around the center of the supercages. The supercages thus form a three-dimensional network with each supercage connected to four other supercages through a 12-membered ring window. The unit cell of Y zeolite consists of eight supercages. Charge-compensating cations can occupy three positions in Y zeolite (see Figure 1). The first type, site I and I′, is located on the hexagonal prism faces between the sodalite units. The second type, site II′ and II, is located in the open hexagonal faces. The third type, site III, is located on the walls of the supercage. In a dry zeolite, site I′, II′, II, and III cations are shielded on one side only; the other side, exposed to the center of the sodalite cage or supercage, remains unshielded. This leads to a partial shielding of the anionic framework of the zeolite as well, and as a consequence electrostatic field gradients are generated extending into the supercage.

Recently, a new approach of selective oxidation of alkanes (ethane, propane, isobutane, and cyclohexane) on cation-exchanged Y zeolite was presented by Frei et al.,[5−8] Grassian et al.,[9] Vanoppen et al.,[10] and our group.[11] The proposed explanation for the selective oxidation, either thermally or photochemically activated, is the confinement of the reactants in a restricted environment (supercage) that exhibits a strong electrostatic field. Complete selectivity was reported due to (1) the diffusional constraints to avoid radical coupling reactions and (2) strong adsorption of partially oxidized products to avoid overoxidation.[9,12−14] Activity was reported to increase in the order NaY < BaY < SrY < CaY caused by the increasing cation electrostatic field.[10,11] It must be stressed that the catalytic cycle has not yet been closed because the oxygenates formed are left adsorbed strongly in the zeolite.

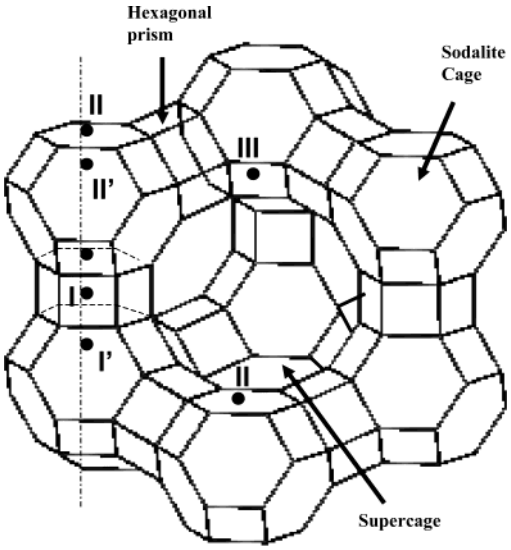

Figure 1. Structure of zeolite Y, where the locations of cation sites I, I′, II, II′, and III are shown.

Our recent results indicated that propane adsorbed via interaction with framework oxygen. Propane adsorption increased with higher basicity of the zeolite lattice oxygen in a series of alkaline-earth-exchanged Y zeolites (i.e., BaY > SrY > CaY > MgY).[11] Moreover, the rate of propane oxidation into

* To whom correspondence should be addressed. E-mail: L.lefferts@utwente.nl. Tel: (+31) 53 4892858. Fax: (+31) 53 4894683.

10.1021/jp048656s CCC: $27.50
Published on Web 09/15/2004

TABLE 1: Chemical Analysis of Zeolite Samples Used in This Study (Determined by XRF)

			chemical composition (wt %)				molar ratio		
zeolite	base material	exchanged with	Al_2O_3	SiO_2	Na_2O	CaO	Na/Al	Ca/Al	exchanged (%)[a]
NaY	NaY		21.47	66.03	12.50		0.96		
CaNaY16	NaY	300 mL of 0.005 M $Ca(NO_3)_2$	21.58	66.17	10.58	1.67	0.81	0.07	16
CaNaY32	NaY	300 mL of 0.01 M $Ca(NO_3)_2$	21.65	66.42	8.41	3.51	0.64	0.15	32
CaNaY45	NaY	300 mL of 0.015 M $Ca(NO_3)_2$	21.61	66.13	6.96	5.31	0.53	0.22	45
CaNaY58	NaY	300 mL of 0.02 M $Ca(NO_3)_2$	21.67	66.25	5.37	6.71	0.41	0.28	58
CaNaY73	NaY	300 mL of 0.05 M $Ca(NO_3)_2$	21.78	66.22	3.44	8.56	0.26	0.36	73
CaNaY90	NaY	300 mL of 0.05 M $Ca(NO_3)_2$ repeated 3 times	21.93	65.83	1.30	10.94	0.1	0.45	90

[a] Exchanged (%) was calculated from the Na content related to the Na content of NaY zeolite.

acetone was influenced not only by the type of metal cations in the zeolite but also by the Brönsted acidity of the zeolite.[11]

For alkaline-earth-exchanged Y zeolites, CaY was observed to have the highest propane and cyclohexane oxidation activity.[10,11] Until now, experiments have been performed exclusively with fully exchanged zeolites. However, sites I, I′, and II′ in cation-exchanged Y zeolite are inaccessible to most organic molecules and even to small molecules such as CO (minimum kinetic diameter is 3.7 Å) and N_2 (minimum kinetic diameter is 3.6 Å), because of the inability to penetrate through a six-membered ring from the supercage into the sodalite cavities.[15] Only cations located on sites II and III are expected to be readily accessible for organic molecules adsorbed within a supercage.[2,16]

On the other hand, cations in the sodalite cages have an effect on the total electrostatic field in the zeolite. Furthermore, the number of Brönsted acid sites varies with cation type; while zeolite NaY can be prepared free of acid sites, this is difficult for fully exchanged CaY zeolite.[11,17] To better understand the role of cations and Brönsted acid sites in the thermal selective oxidation of propane, we investigated the effect of the amount of Ca^{2+} cations on (1) zeolite acidity, (2) propane adsorption, (3) propane selective oxidation, and (4) acetone desorption properties for a series of CaNaY zeolites.

Experimental Section

Materials. The parent material used for this study was a NaY zeolite (Akzo Nobel; sample code, 1122-207) with a Si/Al ratio of 2.6. The CaNaY zeolites were prepared by aqueous ion-exchange of NaY with calcium nitrate solutions of varying concentration (Table 1) under stirring for 6 h at 90 °C. Subsequently, the samples were washed three times with distilled water, filtered, and dried at 100 °C overnight. The chemical composition of the zeolites was analyzed by X-ray fluorescence (XRF) (Table 1). Powder X-ray diffraction gave no indication for collapse of the zeolite structure after activation. ^{27}Al magic-angle spinning (MAS) NMR showed no indication for the formation of extraframework aluminum after activation at 500 °C. Samples are designated CaNaY(xx), with xx representing the Na^+ exchange level as determined from elemental analysis; for example, for CaNaY(70), 70% of Na^+ was exchanged by Ca^{2+}.

Infrared Spectroscopy. The zeolite powder was pressed into a self-supporting wafer and analyzed in situ during adsorption and reaction by means of transmission FTIR spectroscopy using a Bruker Vector22 FTIR spectrometer with a MCT detector. A miniature cell, equipped with CaF_2 transparent windows, which can be evacuated to pressure below 10^{-7} mbar, was used for the in situ experiments. The temperature can be varied from room temperature to 500 °C. Each spectrum consists of 32 scans taken at 4 cm^{-1} resolution.

The samples were activated at 500 °C (ramp, 10 °C/min; dwell, 2 h) in a vacuum ($<10^{-7}$ mbar) and subsequently cooled to 100 and 300 °C for ammonia adsorption. Gas-phase ammonia was introduced into the infrared cell until equilibrium was reached at 1 mbar. Then the system was evacuated, and spectra were recorded. The FTIR spectra were corrected for absorption by the background spectrum.

For propane adsorption and selective oxidation study, the samples were activated in a vacuum ($<10^{-7}$ mbar) at 500 °C (ramp, 10 °C/min) for 2 h, subsequently cooled to 200 °C (dwell 10 h), and cooled to room temperature. Loading of reactants (propane and oxygen) was controlled via the partial pressure. Propane was introduced into the IR cell until equilibrium was reached at 1 mbar in the gas phase, followed by addition of 40 mbar of oxygen. A calibration curve was made by adsorption of known amounts of acetone at room temperature in order to determine the quantity of produced acetone from propane and oxygen. The amount of produced isopropylhydroxide (IHP) was determined by the increase in acetone quantity after thermal conversion of IHP into acetone and water, using an acetone/IHP ratio of 1. The FTIR spectra in propane adsorption and reaction studies were corrected for absorption by the activated zeolite.

Ammonia Temperature-Programmed Desorption Studies (NH_3-TPD). A homemade temperature-programmed desorption (TPD) setup connected to an ultrahigh vacuum (UHV) chamber equipped with a mass spectrometer (Balzers QMG 420) was used for dedicated desorption experiments. After activation at 10^{-3} mbar at 500 °C for 2 h, 60 mg of a sample was exposed to 10 mbar of gas-phase ammonia at 100 °C (to avoid physisorbed NH_3). When the adsorption equilibrium was reached, the sample was evacuated for 1.5 h at 10^{-3} mbar. Then TPD with an increment of 10 °C/min up to 700 °C was started.

Results

Catalyst Characterization. Transmission FTIR spectra of the activated CaNaY zeolites with different Ca^{2+} content are presented in Figure 2. The spectra were calibrated on the amount of sample. All samples exhibited an identical isolated silanol peak at 3744 cm^{-1}, which can be attributed to the outer surface of zeolite crystals or silica impurities.[2,17,18] The absorption band at 3653−3643 cm^{-1} indicated the presence of Brönsted acid sites.[2,17−19] The Brönsted acidity hardly changed with rising calcium content, until sample CaNaY73 from which a clear new band at 3643 cm^{-1} was detected which increased in intensity for CaNaY90. The broad band at 3590 cm^{-1} can be attributed to the $Ca(OH)_x$ species,[11,18,20] and its intensity increased with increasing calcium content. Further, the T-O-T overtone vibrations in the 1700−1900 cm^{-1} region showed a clear shift to higher wavenumber with increasing calcium exchange level, in agreement with the literature.[11,21]

NH_3-TPD was used to differentiate between the number and strength of acid sites in the samples. Figure 3a shows the corresponding TPD profiles on the CaNaY zeolites. For the

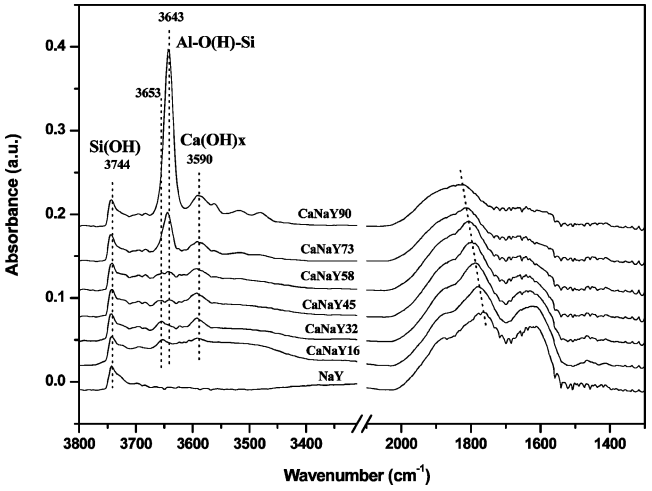

Figure 2. Infrared spectra of activated CaNaY zeolite.

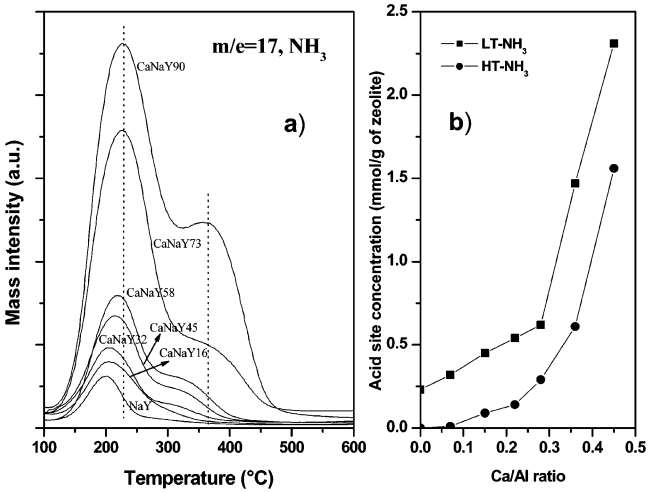

Figure 3. (a) NH_3-TPD profiles of series CaNaY zeolite; (b) adsorbed ammonia concentration of Ca-exchanged Y zeolite as a function of Ca loading.

parent NaY, a small peak at 200 °C was observed, which was previously attributed to aluminum in lattice defect sites.[2] With increasing Ca content, it can be seen from Figure 3a that NH_3 desorbed from at least two types of sites. One type desorbed at low temperature between 150 and 300 °C (LT-NH_3), whereas desorption at higher temperature took place between 250 and 450 °C (HT-NH_3). To evaluate the relative amounts of the LT- and HT-NH_3 peaks, deconvolution was carried out (Figure 3b). High-quality fits were obtained by fitting with only two Gaussian peaks ($r^2 > 0.998$). For both sites, the amount of desorbed ammonia steadily increased until 58% Na^+ was replaced by Ca^{2+}; then a large increase for both sites was observed on CaNaY73 and CaNaY90. Furthermore, the temperature of the maximum of the desorption peaks also gradually shifted to higher values with increasing calcium content.

Although NH_3-TPD clearly showed two desorption sites, these sites cannot automatically be assigned to Brönsted and/or Lewis acid sites, based on TPD only. For this reason, additional infrared experiments on ammonia desorption were carried out. Figure 4b shows the infrared spectra of CaNaY90 after adsorption of ammonia at 100 °C, followed by evacuation for 5 h. In comparison with the infrared spectra of the activated sample (Figure 4a), the band at 3644 cm^{-1} (Brönsted acid sites) disappeared and concurrently new bands at 3400, 3375, 3347, 3280, 1610, and 1464 cm^{-1} appeared. Adsorption of ammonia at 300 °C, followed by evacuation for 1 h at 300 °C (Figure

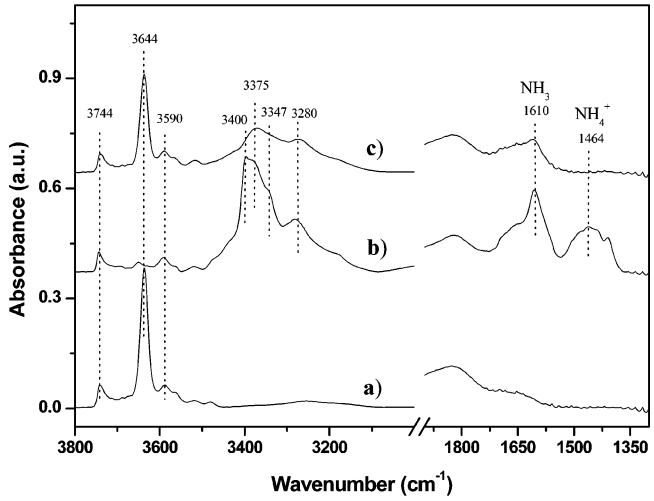

Figure 4. Infrared spectra of (a) activated CaNaY90 zeolite; (b) 1 mbar ammonia adsorbed on CaNaY90 zeolite at 100 °C followed by evacuation for 5 h; (c) 1 mbar ammonia adsorbed on CaNaY90 zeolite at 300 °C followed by evacuation for 1 h.

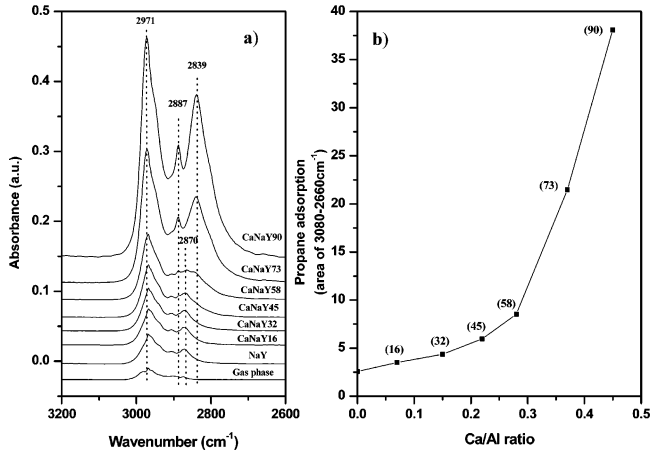

Figure 5. (a) Infrared spectra of 1 mbar propane adsorption on a series of CaNaY zeolites; (b) propane adsorption quantity as a function of the degree of Ca^{2+} content.

4c), resulted in almost complete recovery of the band intensity at 3644 cm^{-1}, and bands at 3375, 3280, and 1610 cm^{-1} decreased but remained. In the literature, the 1464 cm^{-1} peak is normally assigned to ammonium cations arising from the protonation of ammonia on Brönsted acid sites, while the band at 1610 cm^{-1} is attributed to ammonia bonded to Lewis acid sites.[22,23]

The infrared spectra in Figure 4 clearly show that ammonia adsorbed on both Brönsted and Lewis acid sites at 100 °C, while only adsorption on Lewis acid sites occurred at 300 °C. Further, from comparison of the infrared spectra in Figure 4 it follows that the bands at 3400 and 3347 cm^{-1} are due to N−H stretch vibrations of NH_4^+, since they appear together with the band at 1464 cm^{-1} and they are not present when the O−H stretch vibration of the Brönsted acid sites is observed at 300 °C (Figure 4c). The peaks at 3375 and 3280 cm^{-1} belong to the N−H stretch vibration of NH_3 adsorbed at Lewis acid sites, since they appear together with the band at 1610 cm^{-1}, even at 300 °C. Since no change in intensity at 3744 and 3590 cm^{-1} was found after adsorbed ammonia, it can be concluded that ammonia did not adsorb on Si−OH or $Ca(OH)_x$ species.

Propane Adsorption on CaNaY. Figure 5a presents the FTIR spectra of adsorbed propane at 1 mbar pressure of propane on CaNaY at room temperature. The band at 2971 cm^{-1} steadily

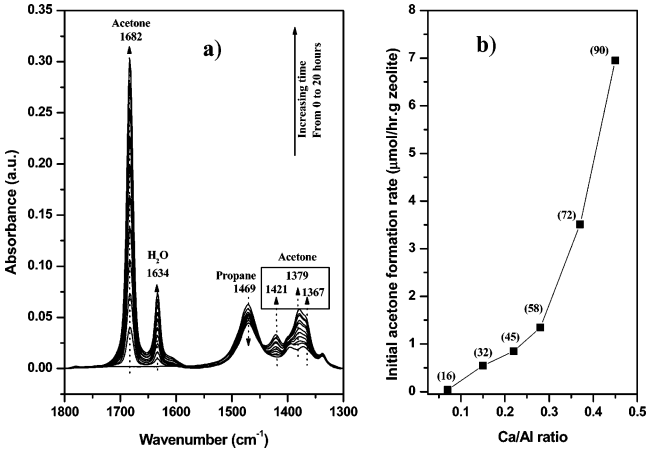

Figure 6. (a) Infrared spectra of CaNaY73 zeolite after loading 1 mbar propane and 40 mbar oxygen at room temperature as a function of time; (b) initial acetone formation rate of propane oxidation as a function of the degree of Ca^{2+} content (the initial rate was calculated from data of the first 2 h of reaction).

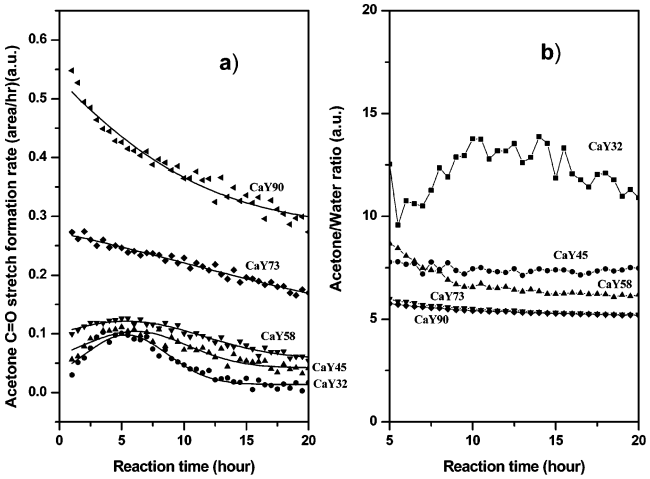

Figure 7. (a) Acetone C═O stretch formation rate as a function of time for propane oxidation on CaNaY zeolite; (b) acetone/water ratio as a function of time for propane oxidation on series CaNaY zeolites.

increased with higher calcium content. Interestingly, from CaNaY58 new bands at 2839 and 2887 cm^{-1} appeared, whose intensities increased with increasing calcium exchange. Figure 5b displays the propane uptake (interpreted as the integrated area between 3080 and 2660 cm^{-1}) as a function of the degree of Ca^{2+} content. A small increase in the propane adsorption was found below 58% of Na^+ exchange, while a considerable increase in the amount of adsorbed propane was observed for higher calcium contents.

Propane Oxidation on CaNaY Zeolites. After loading 1 mbar propane and 40 mbar oxygen on activated CaNaY73 zeolite, infrared spectra showed reactant depletion and product formation as a function of time (Figure 6a). The developing absorptions can be completely attributed to acetone (1682, 1421, 1379, and 1367 cm^{-1}) and water (1634 cm^{-1}).[5,11]

The initial acetone formation rate (calculated from data of the first 2 h of reaction) as a function of the degree of Ca^{2+} content is displayed in Figure 6b. As expected, the reaction rate increased when increasing the zeolite Ca^{2+} content. However, a dramatic increase in the reaction rate was observed from CaNaY58 up to CaNaY90.

Figure 7a shows the acetone formation rate as a function of time, based on the integrated area of the acetone $\nu_{C=O}$ infrared absorption peak. While for CaNaY73 and CaNaY90 the rate is

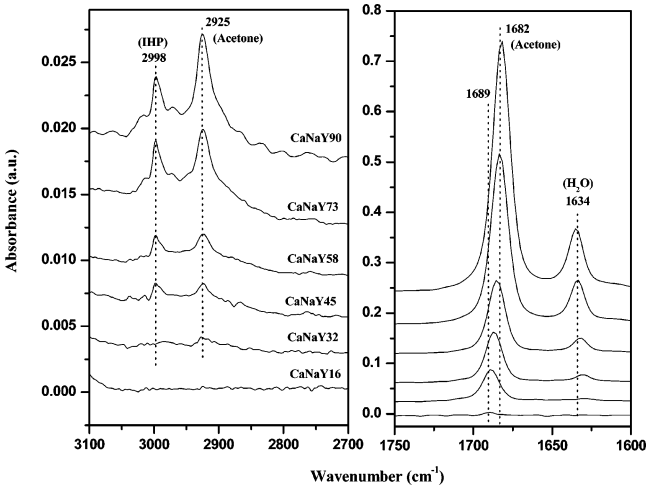

Figure 8. Infrared spectra after 20 h of reaction, followed by 5 min of evacuation.

observed to decrease in time, the samples with lower calcium content clearly show a maximum in activity. Figure 7b displays the fluctuation of the acetone-to-water ratio as a function of time. It was found that the ratio of acetone to water decreased with increasing Ca^{2+} content until 73% of Na^+ was replaced. For CaNaY16, no significant water signal was observed in the infrared spectrum after 20 h of reaction.

After 20 h of reaction and removal of adsorbed propane via evacuation, bands at 2998 and 2925 cm^{-1} were detected that previously were masked by propane (Figure 8), which were attributed to IHP and acetone, respectively.[7,11] Decomposition of IHP at 200 °C has been reported to form acetone and water exclusively.[14] Therefore, all evacuated samples were further heated at 200 °C and followed with FTIR (not shown). It was found that about 7% for CaNaY90, 9% for CaNaY73, 14% for CaNaY58, and 11% for CaNaY45 of additional acetone was produced from the converted IHP compared to the acetone amount at the beginning of these experiments. No acetone was formed on CaNaY32 and CaNaY16 when heating the samples, which agrees with the fact that no IHP was detected after propane oxidation (Figure 8). Further, a clear shift in the acetone C═O stretch frequency was observed from 1689 cm^{-1} for CaNaY16 to 1682 cm^{-1} for CaNaY90. In addition, the water-bending mode shows a small shift to higher wavenumber with increasing calcium content. Both observations have been explained by a difference in adsorption sites: water adsorbs close to the Ca^{2+} cations, while acetone is associated with the Brönsted sites in the samples,[11,14] which will be discussed in the following section.

It has been discussed in our previous paper[11,14] that propane partial oxidation to acetone on alkaline-earth-exchanged Y zeolite proceeds via IHP as a reaction intermediate, which results in the overall reaction

$$CH_3CH_2CH_3 + O_2 \rightarrow CH_3C(OOH)HCH_3 \rightarrow CH_3COCH_3 + H_2O$$

The present and previous results showed that the molar ratio of [IHP]/[acetone] was in the range of 0.07 and 0.14 after 20 h of reaction for all CaNaY zeolites studied.[14] Consequently, it can be concluded that the IHP decomposition into acetone is considerably faster than the IHP formation on CaNaY zeolite. Therefore, the rate of acetone formation can reasonably be assumed to reflect the propane conversion rate in this work.

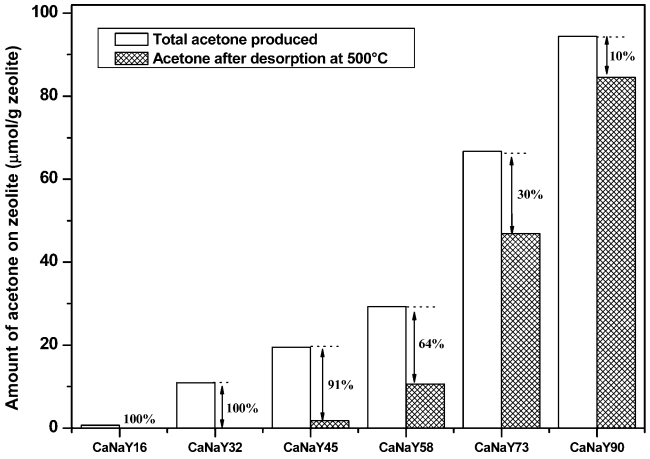

Figure 9. Desorption of acetone after TPD experiments.

Acetone Desorption from CaNaY Zeolites. After 20 h of reaction and subsequently 1 h of evacuation, no desorbed products were detected by on-line mass spectrometry. For this reason, TPD was applied to attempt to remove the remaining adsorbed molecules (rate, 10 °C/min; up to 500 °C; dwell, half hour). At the end of the TPD experiment, the samples were cooled to room temperature and infrared data were taken. Figure 9 displays the acetone desorption quantity for the series of CaNaY zeolites based on the acetone C═O band intensity at 1689−1682 cm^{-1} before and after the TPD.[14] It can be clearly seen that the relative amount of desorbed acetone increased with decreasing Ca^{2+} content. No new bands were observed in the infrared spectra during desorption, thus excluding the conversion of acetone into other products. During TPD also mass spectra were taken to detect gas-phase compounds. Acetone and water were detected exclusively, and no other oxidation or dimerization products could be detected.

Discussion

Several characteristics of the CaNaY zeolite samples changed in parallel with increasing the Ca^{2+}-exchange level: (1) the FTIR intensity of Brönsted acid sites and $Ca(OH)_x$ species increased (Figure 2), (2) the amount of desorbed ammonia (Figure 3) from Brönsted and Lewis acid sites increased, (3) the adsorbed propane quantity increased (Figure 5), (4) the initial acetone formation rate increased (Figure 6), and (5) the amount of desorbed acetone after TPD decreased (Figure 9).

Furthermore, all these properties show a sudden change from CaNaY58 to higher Ca^{2+} amounts, which can be explained by the location of Ca^{2+} in the supercage of the Y-zeolite framework as will be explained below. In a typical fully dehydrated NaY zeolite, the distribution of Na^+ ions in each unit cell is 30 ions located in site I, 20 ions located in site I′, and 8 ions located in site II (see Figure 1).[24] After a full exchange with Ca^{2+}, single-crystal X-ray analysis showed that the Ca^{2+} ions in a completely dehydrated Y zeolite are distributed according to 14 ions in site I, 4 ions in site I′, and 11 ions in site II per unit cell.[25] This would suggest that roughly 40% of the Ca^{2+} ions are located in the supercages, in the case of complete exchange.

A marked change in the adsorption of CO and CO_2 on CaNaY zeolite has been reported when the degree of calcium exchange exceeds about 50% and 46%, respectively.[19,27] This agrees well with the observations in this study (Figure 3 and Figure 5). The results with CO and CO_2 have been explained based on the location of Ca^{2+} in the supercage, since the CO and CO_2 molecules cannot pass the six-membered ring to reach the sodalite cages, like propane in this study. The slight inconsistency between the single-crystal X-ray study, suggesting about 40% of the Ca^{2+} ions in the supercage, and the interpretation of the adsorption studies, suggesting 50% of the Ca^{2+} ions in the supercage, might be due to differences in the activation temperature[26] or to changes in the Ca^{2+} siting induced by the adsorption of molecules such as CO, CO_2, and propane.

At lower exchange levels, the Ca^{2+} cations occupy preferably the energetically most favorable sites, that is, site I in the hexagonal prisms.[27] In this site, the cations are fully surrounded by lattice oxygen, causing maximal screening of the positive charge. When the exchange level is increased, the additional cations are located in sites I′ and II, somewhat displaced from the centers of the two types of six-numbered rings in the sodalite unit. These cations are shielded by lattice oxygen at one side only, while at the other side the cation is exposed to the center of the sodalite cage or supercage, respectively.[25] These partially shielded charge centers generate an electrostatic field extending into the zeolite cages. The shielding is especially limited for cations facing a supercage. Therefore, site I positions are occupied first by Ca^{2+} ions; however, Jacobs et al. concluded that a small fraction of the Ca^{2+} ions start to occupy supercage positions before the hexagonal prisms are completely occupied.[19]

Brönsted and Lewis Acidity. It is generally accepted that in divalent-cation-exchanged Y zeolites, the strong electrostatic field of M^{2+} cations on water molecules can result in a dissociation of these molecules according to refs 17 and 20: $Ca^{2+} + H_2O(ad) \rightarrow Ca(OH)^+ + H^+$. The protons are fixed to lattice oxygen atoms and account for the hydroxyl vibration at 3653−3643 cm^{-1}. The hydroxyl vibration at 3590 cm^{-1} results from the $Ca(OH)_x$ species (Figure 2). The higher electrostatic field of supercage Ca^{2+} ions results in a sharp increase in Brönsted acidity as observed in the FTIR spectra (Figure 2).

Combination of the infrared results in Figure 4 with the TPD results in Figure 3 leads to the conclusion that the HT-NH_3 peak can be attributed to ammonia desorbing from Lewis acid sites. The LT-NH_3 peak should be assigned to both Brönsted acid sites and Lewis acid sites, since NH_3 adsorption at 100 °C results in IR signals (Figure 4) attributed to ammonia on both types of sites. Most likely, for all samples also a small amount could be adsorbed on aluminum defect sites as was observed for the parent NaY; however this peak could obviously not be separated from the LT-NH_3 peak in Figure 3.

Three different sources for Lewis acid sites in CaNaY zeolites might contribute: (1) structural defects in the framework, (2) extraframework aluminum, and (3) bare Ca^{2+} ions. ^{27}Al MAS NMR, however, showed no extraframework aluminum. Moreover, for USY zeolites it was shown that NH_3 desorbed at lower temperatures from aluminum Lewis acid sites than from Brönsted acid sites, that is, below 200 °C.[22] Consequently, the high-temperature desorption peak arises from bare Ca^{2+} cations. For Ca^{2+}- and Sr^{2+}-exchanged X zeolites, it was observed by X-ray diffraction that ammonia adsorbed exclusively on Ca^{2+} and Sr^{2+} located in the sodalite and supercage.[30,31] In fully exchanged CaY zeolite, only a very small fraction of Ca^{2+} (4 of in total 29 cations) is located in the sodalite cage (site I′).[26] For this reason, we conclude that the HT-NH_3 peak mainly is originating from supercage Ca^{2+} ions.

The bare metal cations in Y zeolite play an essential role in selective oxidation of alkanes.[11,14] It is not yet clear how many Ca^{2+} ions in the supercage position are converted to $Ca(OH)_x$ species. This is currently under investigation.

Propane Adsorption. Figure 10a shows the amount of adsorbed propane normalized to the total number of Ca^{2+} ions in the zeolites. It clearly demonstrates that propane adsorption

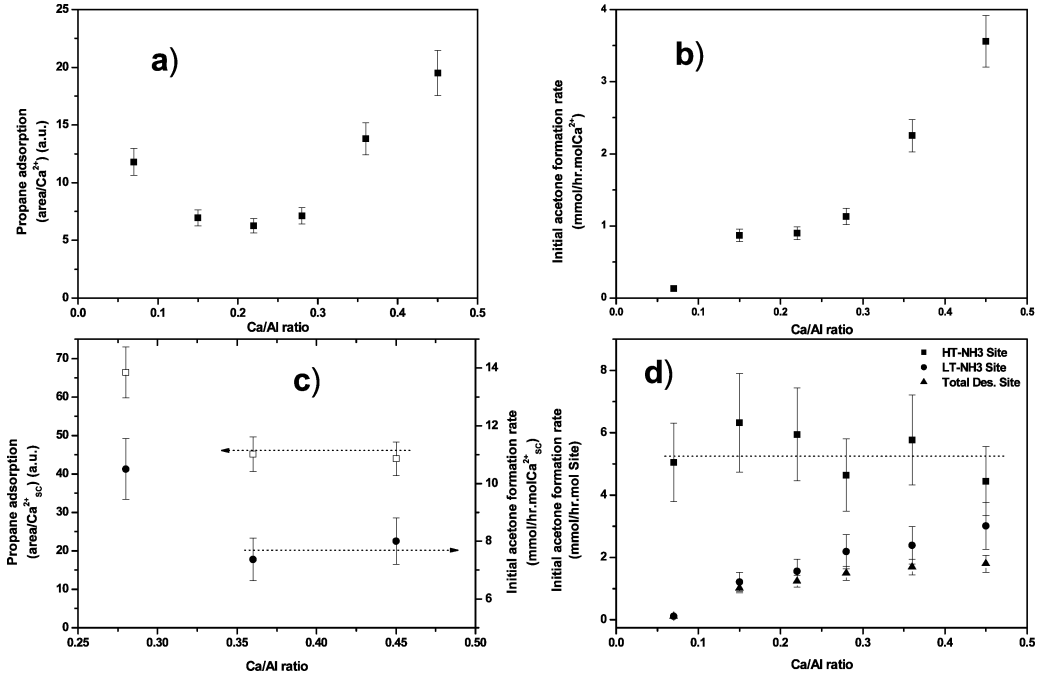

Figure 10. (a) Propane adsorption (FTIR band area between 3100 and 2700 cm^{-1}) per Ca^{2+} as a function of Ca^{2+} content; (b) initial rate of formation of acetone per Ca^{2+} during propane oxidation as a function of Ca^{2+} content; (c) propane adsorption and initial acetone formation rate per Ca^{2+} in the supercage (SC) as a function of Ca^{2+} content; (d) initial acetone formation rate per ammonia desorption site as a function of Ca^{2+} content.

per Ca^{2+} decreased with increasing Ca^{2+} content until 50% of Na^+ was replaced by Ca^{2+}; subsequently the propane adsorption per Ca^{2+} increased rapidly. The largest contribution to the total integrated area of propane ν_{C-H} vibrations originates from the peak at 2839 cm^{-1}, which was only visible from CaNaY58 to CaNaY90 (Figure 5a). Hydrocarbon adsorption in zeolites has been reported to be due to enhanced interaction with framework oxygen; however the bonding of alkanes in zeolites is known to be influenced as well by polarization of saturated hydrocarbons at cations. Normally, the latter contribution is smaller than the enhanced interaction from the close fit of the adsorbate molecules within zeolite cages or channels.[3,28,29] The C−H vibration at 2839 cm^{-1} on CaNaY58, -73, and -90 (Figure 5a) indicates a significant interaction between propane and the zeolite. Further, molecules such as propane (minimum kinetic diameter, 4.3 Å) are too big to penetrate the six-membered rings (about 2.5 Å in diameter) to enter the sodalite cages and the hexagonal prisms;[2] propane thus adsorbs in the supercages exclusively. The sudden and linear increase in the amount of adsorbed propane per Ca^{2+} from CaNaY58 up to CaNaY90 strongly suggests this is due to Ca^{2+} cations in the supercages, which induce both a cation−dipole interaction and an increasing basicity of nearby lattice oxygen ions, since supercage Ca^{2+} cations cannot shield lattice charges equally well as monovalent Na^+ ions.

Propane Oxidation. For CaNaY32, CaNaY45, and CaNaY58, activation was observed in the first hours of reaction, accompanied by a high acetone-to-water ratio compared to CaNaY73 and CaNaY90 (Figure 7). In a previous paper, we explained these phenomena by the hydrolysis of produced water on zeolites with low initial Brönsted acidity.[11] Hydrolysis leads to higher acidity, which favors decomposition of IHP into acetone, resulting in a higher acetone-to-water ratio. Further, the presence of water in the zeolite will inevitably reduce the electrostatic field resulting in deactivation as observed for all samples. The fact that no activation curve was observed for CaNaY73 and CaNaY90 suggests that the rate of deactivation is higher than the rate of activation, which is probably due to the larger amounts of water formed in the initial stage. Moreover, these samples already have significant Brönsted acidity, which limits the possibility for additional hydrolysis of produced water. Therefore the acetone-to-water ratio is smaller.

Figure 10b shows the normalized initial acetone formation rate per Ca^{2+} cation in the zeolites. Clearly, a sudden linear increase is observed with calcium levels above 50% exchange, similar to the amount of adsorbed propane (Figure 10a). Assuming that from the 50% exchange level up, the cations fill up sites in the supercages, the adsorbed propane quantity and initial oxidation rate per supercage-Ca^{2+} were calculated for CaNaY58, CaNaY73, and CaNaY90 (Figure 10c). A constant propane quantity and oxidation rate per supercage-Ca^{2+} ion were found within experimental error for CaNaY73 and CaNaY90. For CaNaY58, the calculated numbers are slightly higher (1.15 times) compared to CaNaY73 and CaNaY90. Since the CaNaY58 sample is just above the 50% exchange level, only a minority of Ca^{2+} cations would be in the supercage based on the assumption. The result here indicates that approximately 15% more Ca^{2+} ions are located in the supercage. This is also in agreement with the observation that both CaNaY32 and CaNaY45 show some propane oxidation activity. Since propane cannot enter the sodalite cages or hexagonal prisms, this activity is likely to be due to a few cations located in the supercages. Our observations agree with the conclusion of Jacobs et al.[19] that although preferential filling of site I positions by Ca^{2+} takes place, some Ca^{2+} ions occupy supercage positions before the hexagonal prisms are completely occupied.

To test our assumption, the initial acetone formation rate per Lewis acid site, as obtained from the NH_3-TPD experiments, was calculated (Figure 10d). For comparison, also the normalized activity per Brönsted acid site and total number of acid sites are given in Figure 10d. Clearly, only for the Lewis acid sites was a similar activity per site found for all CaNaY zeolites. Since the Lewis sites were identified as bare Ca^{2+} supercage cations (see above), this confirms that only Ca^{2+} cations in the

supercage contribute almost exclusively to propane oxidation activity at room temperature.

Acetone Desorption. Finally, Figure 9 shows that the relative amount of desorbed acetone decreases with higher Ca^{2+} exchange level, even though the acetone coverage was higher. Furthermore, the shifts to lower wavenumber in the infrared spectra for both the Brönsted OH frequency and the C═O stretch frequency of acetone with increasing calcium content are similar (Figures 2 and 8), which suggests that acetone is adsorbed on the Brönsted acid sites. The present results are in agreement with previous observations on different alkali-earth-exchanged Y zeolites, that the relative amount of desorbed acetone decreased with increasing Brönsted acidity.[14] Obviously, acetone is well stabilized in zeolites with high contents of Ca^{2+} and Brönsted acid sites. At present, it is not yet clear whether Brönsted acid sites also affect the IHP formation or whether Ca^{2+} cations influence the acetone adsorption state; this is currently under investigation.

Conclusion

Increasing the Ca^{2+} exchange level in CaNaY zeolites results in altered properties for the zeolites: the amount of Brönsted and Lewis acid sites increased, the adsorbed propane quantity increased, the initial acetone formation rate increased, and the amount of desorbed acetone decreased. Moreover, all these properties showed a sudden change above 50% Na^+ exchange levels with Ca^{2+}, which can be fully attributed to the location of Ca^{2+} in the Y-zeolite framework. Clearly, only Ca^{2+} ions located in the supercage contribute to the formation of Brönsted and Lewis acidity as well as propane oxidation activity at room temperature.

Acknowledgment. This work was performed under the auspices of The Dutch Institute for Research in Catalysis (NIOK). We thank Raquel Rios Font for help in catalysis preparation, P. C. M. M. Magusin for the ^{27}Al NMR measurements, J. A. M. Vrielink for the XRF measurements, and Bert Geerdink for the technical support. The financial support from CW/STW Project No. 790-36-057 is gratefully acknowledged.

References and Notes

(1) Barthomeuf, D. *Catal. Rev.—Sci. Eng.* **1996**, *38*, 521−613.

(2) Breck, D. W. *Zeolite molecular sieves*: *Structure, chemistry, and use*; Wiley: New York, 1974.

(3) van Bekkum, H. *Introduction to zeolite science and practice*; Elsevier: Amsterdam, 2001.

(4) Bhatia, S. *Zeolite catalysis*: *Principles and applications*; CRC Press: Boca Raton, FL, 1990.

(5) Sun, H.; Blatter, F.; Frei, H. *Catal. Lett.* **1997**, *44*, 247−253.

(6) Sun, H.; Blatter, F.; Frei, H. *J. Am. Chem. Soc.* **1996**, *118*, 6873−6879.

(7) Blatter, F.; Sun, H.; Frei, H. *Chem.—Eur. J.* **1996**, *2*, 385−389.

(8) Sun, H.; Blatter, F.; Frei, H. *Abstr. Pap.—Am. Chem. Soc.* **1996**, *211*, 3-ORGN.

(9) Larsen, R. G.; Saladino, A. C.; Hunt, T. A.; Mann, J. E.; Xu, M.; Grassian, V. H.; Larsen, S. C. *J. Catal.* **2001**, *204*, 440−449.

(10) Vanoppen, D. L.; DeVos, D. E.; Jacobs, P. A. *Prog. Zeolite Microporous Mater., Part A−C* **1997**, *105*, 1045−1051.

(11) Xu, J.; Mojet, B. L.; Ommen, J. G. v.; Lefferts, L. *Phys. Chem. Chem. Phys.* **2003**, *5*, 4407−4413.

(12) Blatter, F.; Sun, H.; Vasenkov, S.; Frei, H. *Catal. Today* **1998**, *41*, 297−309.

(13) Frei, H. *World Congr. Oxid. Catal., Proc., 3rd* **1997**, *110*, 1041−1050.

(14) Xu, J.; Mojet, B. L.; Ommen, J. G. v.; Lefferts, L. *J. Phys. Chem. B* **2004**, *108*, 218−223.

(15) Bordiga, S.; Scarano, D.; Spoto, G.; Zecchina, A.; Lamberti, C.; Otero Arean, C. *Vib. Spectrosc.* **1993**, *5*, 69.

(16) Ramamurthy, V.; Lakshminarasimhan, P.; Grey, C. P.; Johnston, L. J. *Chem. Commun.* **1998**, 2411−2424.

(17) Ward, J. W. *J. Phys. Chem.* **1968**, *72*, 4211−4223.

(18) Ward, J. W. *J. Catal.* **1968**, *10*, 34−46.

(19) Jacobs, P. A.; Cauwelaert, F. H.; Uytterhoeven, J. B. *J. Chem. Soc., Faraday Trans. 1* **1972**, *68*, 1056−1068.

(20) Uytterhoeven, J. B.; Schoonheydt, R. *J. Catal.* **1969**, *13*, 425−434.

(21) Sponer, J. E.; Sobalik, Z. *J. Phys. Chem. B* **2001**, *105*, 8285−8290.

(22) Miessner, H.; Kosslick, H.; Lohse, U.; Parlitz, B.; Tuan, V.-A. *J. Phys. Chem.* **1993**, *97*, 9741−9748.

(23) Nakamoto, K. *Infrared Spectra of Inorganic and Coordination Compounds*; Wiley-Interscience: New York, 1986.

(24) Eulenberger, G. R.; Shoemaker, D. P.; Keil, J. G. *J. Phys. Chem.* **1967**, *71*, 1812−1819.

(25) Bennett, J. M.; Smith, J. V. *Zeolites* **1968**, *3*, 633−642.

(26) Costenoble, M. L.; Mortier, W. J.; Uytterhoven, J. B. *J. Chem. Soc., Faraday Trans. 1* **1977**, *73*, 466−476.

(27) Egerton, T. A.; Stone, F. S. *Trans. Faraday Soc.* **1970**, *66*, 2364−2377.

(28) Janchen, J.; Mortier, W. J. *J. Phys. Chem.* **1996**, *100*, 12489−12493.

(29) Smit, B. *J. Phys. Chem.* **1995**, *99*, 5597−5603.

(30) Jang, S. B.; Jeong, M. S.; Kim, Y.; Song, S. H.; Seff, K. *Microporous Mesoporous Mater.* **1999**, *28*, 173−183.

(31) Jang, S. B.; Jeong, M. S.; Kim, Y.; Song, S. H.; Seff, K. *Microporous Mesoporous Mater.* **1999**, *30*, 233−241.